Dyes and Pigments 132 (2016) 7–19

Contents lists available at ScienceDirect

Dyes and Pigments

journal homepage: www.elsevier.com/locate/dyepig

Synthesis and systematic evaluation of symmetric sulfonated centrally C–C bonded cyanine near-infrared dyes for protein labelling

Steffen van der Wal [a, 1], Joeri Kuil [b, c, 1], A. Rob P.M. Valentijn [b], Fijs W.B. van Leeuwen [a, d, *]

[a] Interventional Molecular Imaging Laboratory, Department of Radiology, Leiden University Medical Center, The Netherlands
[b] Department of Clinical Pharmacy and Toxicology, Leiden University Medical Center, The Netherlands
[c] Department of Surgery, Leiden University Medical Center, The Netherlands
[d] Laboratory of BioNanoTechnology, Wageningen University, The Netherlands

ARTICLE INFO

Article history:
Received 22 January 2016
Received in revised form
15 March 2016
Accepted 16 March 2016
Available online 20 April 2016

Keywords:
Stacking
Stability
Conjugation
Fluorescence
Image guided surgery

ABSTRACT

The most commonly used near-infrared cyanine dyes contain an aryl ether that is not fully stable towards nucleophiles. Replacement of the aryl ether by a more stable carbon-carbon bond can improve the stability. In this work we have synthesized a series of four negatively-charged symmetrical C–C bond-containing Cy7 derivatives and compared them to the known dyes indocyanine green (ICG) and IRDye 800CW. The extent of stacking of these C–C bond-containing dyes was higher than reported for aryl ether dyes, but stacking could be minimized by altering the surface charge of the molecules and by introducing sulfonate groups. Furthermore, the degree of stacked dye in an antibody-dye conjugate was similar to the degree of stacking of free dye under labeling conditions. In our view, C–C bond-containing Cy7 dyes provide a chemical platform, based on which one can improve the photophysical properties and stacking behavior, thereby generating interesting additions to the conjugation toolbox available for e.g. antibodies.

1. Introduction

Fluorescent dyes have been extensively used in biomedical research [1]. Due to the fact that in the far-red and near-infrared (NIR) region of the light spectrum the tissue penetration of light is higher [2], and the fact that at these wavelengths auto-fluorescence of endogenous tissues is relatively low, in general such dyes are preferred for in vivo imaging [3]. NIR dyes are most often used to conjugate to e.g. antibodies that target tumor biomarkers and as such help to visualize specific tissue types, such as tumour tissue [4,5].

Currently, the only EMA- and FDA-approved NIR fluorescent dye is indocyanine green (**ICG**). This dye belongs to the class of cyanine dyes and can be effectively considered a Cy7.5 derivative. The prefix 7 is added since it has seven carbon atoms (methine moieties) between the benzoindolenine groups. The suffix 0.5 is added because **ICG** contains benzoindolenine groups instead of indolenine, giving a further red-shift (approx. 40 nm) in the absorption and emission spectra. Cy-dyes in general are characterized by good chemical- and photo-stability, exceptional molar extinction coefficients and good quantum yields, resulting in a high brightness [6]. The brightness of **ICG**, however, is lower than that of similar Cy7 derivatives or far-red Cy-dyes [1].

ICG displays a low solubility in salt-containing buffers and has a high tendency to form stacking-aggregates. The stacking behavior of **ICG** has been described in great detail by Landsman et al. [7], who showed extensive concentration-dependent dye aggregation in salt-containing buffer and, to a lesser extent, in water. Due to alignment of dipole moments, the aggregates display an altered absorption maximum. H-aggregates, which display side-by-side dipole alignments (Fig. 1), tend towards shorter wavelengths (a hypsochromic shift) and display a very low fluorescence intensity [8]. Other types of aggregates, called J-aggregates, display a red-shifted absorption maximum (a bathochromic shift) and occur when the orientation of the dipoles is more head-to-tail (Fig. 1) [8]. These J-aggregates of dyes also show distinct fluorescence properties, characterized by a very low Stokes shift [9]. Dye stacking is not unique to **ICG** and has been described for a great variety of cyanine and cyanine-like dyes [10,11].

The low water solubility of **ICG** drives the stacking and

* Corresponding author. Albinusdreef 2, 2333 ZA Leiden, The Netherlands.
E-mail address: F.W.B.van_leeuwen@LUMC.nl (F.W.B. van Leeuwen).
[1] Authors contributed equally.

http://dx.doi.org/10.1016/j.dyepig.2016.03.054
0143-7208/

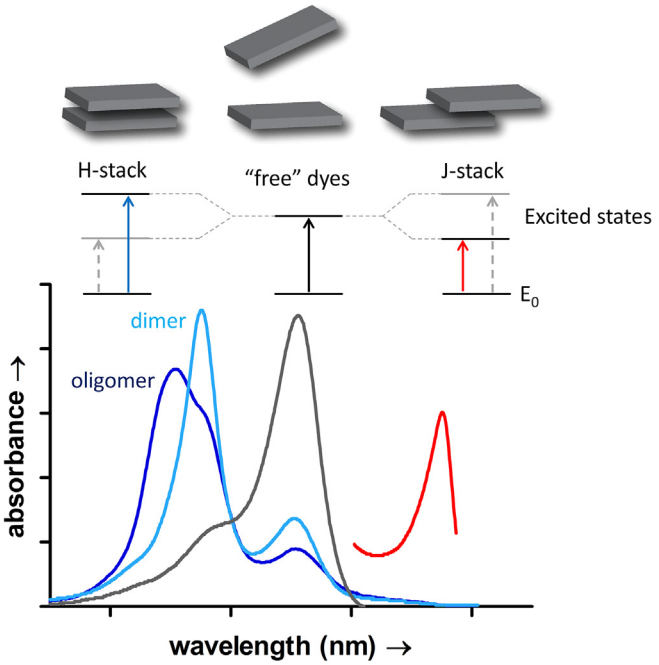

Fig. 1. Schematic representation of stacking of Cy7 derivatives (dyes depicted as gray blocks) as blue-shifted H-aggregates and red-shifted J-aggregates. Example absorption spectra are taken from the spectra below in this manuscript. Spectroscopically forbidden transitions are depicted as gray arrows while spectroscopically allowed transitions are depicted in colored arrows [17]. (For interpretation of the references to color in this figure legend, the reader is referred to the web version of this article.)

aggregation behavior. This same effect causes binding of **ICG** to hydrophobic domains of proteins. The interaction of **ICG** with albumin proteins has been widely used in chromatography and was more recently used to non-covalently functionalize a clinically approved radiotracer based on colloidal albumin [12,13]. The resulting ICG-^{99m}Tc-nanocolloid complex proved stable in the lymphatic system and has been successfully applied in the clinic to obtain surgical guidance towards sentinel lymph nodes [14,15].

As it lacks an appropriate functional group for conjugation such as a carboxylic acid, **ICG** itself cannot be used for covalent labelling of proteins or other molecules (see Fig. 2). However, because of its widespread clinical use, **ICG** functions as (photo)physical benchmark for near infrared dyes. Alternative NIR dyes containing a carboxylic acid have been synthesized for use in bioconjugations [4]. Example are the dyes **ZW800-1** [16] (symmetric; Fig. 2), **ICG-OSu** [5], and **IRDye 800CW** (non-symmetric; Fig. 2).

Zhou et al. showed that during protein conjugation the dye **ICG-OSu**, especially at higher degrees of labelling, yielded a high percentage of stacked dye on the conjugate [5]. This effect was also described by others [18] and was found to be strongly dependent on the structure of the dye [19,20]. An analogous phenomenon can also occur during the non-covalent assembly on structures such as polymers [21]. Dye stacking of both H- and J-type on conjugates are undesirable, as these structures diminish the overall brightness. Moreover, as the overall chemical structure of an imaging agent dictates its in vivo kinetics, having (multiple) stacked dyes on one targeting agent can influence its properties [22], especially when smaller proteins, such as nanobodies are used [23]. Prevention of stacking thus seems critical for future developments.

The class of aryl ether-containing cyanine dyes, of which **IRDye 800CW** and **ZW800-1** are the most prominent examples, possess exceptional photophysical properties and depending on their structure, exhibit less stacking compared to **ICG**. Despite this, **ZW800-1** and several other aryl ether-containing dyes are known to be unstable towards nucleophilic attack by amines and thiols [24–27], resulting in a substitution of the aryl ether by the nucleophile with release of the phenol moiety. This phenol may contain the carboxylic moiety used for conjugation to targeting moieties in the case of symmetric dyes. While the resulting dye substituted by an amine has different photophysical properties, the thiol substitution product has similar photophysical properties to the parental dye [28]. **IRDye 800CW** contains the same (unstable) ether bond and could theoretically possess a similar instability. Due to the location of the carboxylic acid on the N-alkyl substituent of **IRdye 800CW**, cleavage of the ether bond would not lead to dissociation of the dye from its targeting moiety in this dye as opposed to symmetrical aryl ether dyes (**ZW800-1**).

Achilefu and co-workers have described an elegant approach towards more stable analogues of these aryl ether dyes, that lack the labile aryl ether bond itself but did not describe the stacking behavior of these dyes in detail [29,30]. Later, this approach has also been used to generate analogues of **ZW800-1** by two different groups resulting in the structurally similar stabile dyes **ZWCC** [24] and **ZW800-1C** [25] with excellent photophysical properties. Unfortunately, when investigated in more detail these dyes were found to possess reduced solubility and display an increase in the amount of stacking.

In an attempt to provide more fundamental insight in the structure activity relation of symmetric Cy7 derivatives, we set out to synthesize a systematic series of negatively charged symmetrical sulfonate-containing dyes. These dyes lack the zwitterionic

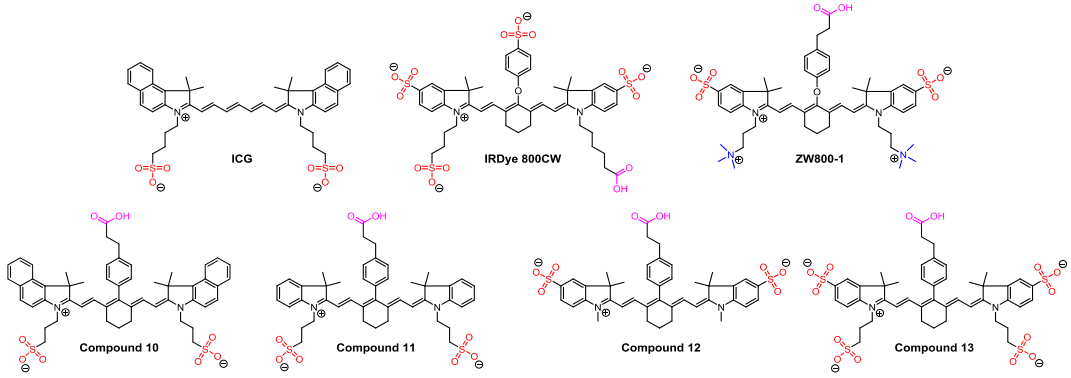

Fig. 2. Top row: Structures of various NIR dyes with sulfonate groups in red, trimethyl ammonium groups in blue and carboxylic acids used for conjugation purposes in purple. Bottom: the four dyes synthesized and evaluated in this work. (For interpretation of the references to color in this figure legend, the reader is referred to the web version of this article.)

character of **ZWCC** and **ZW800-1C** that in itself may lead to increased stacking through coulombic interactions. They also incorporate the stable core of earlier reported dye analogues, with varying charge density, lipophilicity and positioning of the negatively charged sulfonate groups (see Fig. 2 bottom row) [24,25,29]. The stacking behavior of the dyes in solution and in monoclonal antibody conjugates, along with their chemical stability and photophysical properties were compared to the well-known conjugatable dye **IRDye 800CW** and the (photo)physical reference compound **ICG**.

2. Experimental

2.1. Materials and reagents

Potassium 2,3,3-trimethyl-*3H*-indole-5-sulfonate [31] and Vilsmeijer-Haack reagent **1** [31] were synthesized according to published procedures. **IRDye 800CW** (as N-hydroxysuccinimide ester and as carboxylic acid) was obtained from LI-COR (Lincoln NE, USA). Trastuzumab (Herceptin) was obtained from Roche. All other chemicals were obtained from commercial sources and used without further purification. Preparative HPLC was performed on a Waters Prep LC 4000 system using a 2487 dual wavelength absorbance detector, a Fraction Collector III and a flow rate of 25 mL/min (Dr. Maisch Reprosil-Pur C18-AQ 120 Å 10 μm (100 × 20 mm) column). Analytical HPLC was performed on a Waters Acquity UPLC-MS system using a Acquity UPLC photodiode array detector, an SQ Detector mass spectrometer and a flow rate of 0.5 mL/min (Waters BEH C18 130 Å 1.7 μm (100 × 2.1 mm) column). Lyophilisation was performed with a Steris GT4 lyophilizer. NMR spectra were taken using a Bruker DPX-300 spectrometer (^{1}H NMR) or a Bruker Avance III 600 MHz apparatus equipped with a Cryo platform (^{13}C NMR) and the chemical shifts are given in ppm (δ) relative to DMSO-d6 (2.50 ppm and 39.52 ppm for ^{1}H and ^{13}C respectively). Abbreviations used include singlet (s), doublet (d), triplet (t) and unresolved multiplet (m). HRMS spectra were taken using a Thermo LTQ-FT Ultra mass spectrometer using the negative ion mode.

2.2. Synthesis

2.2.1. 3-(1,1,2-trimethyl-1H-benzo[e]indol-3-ium-3-yl)propane-1-sulfonate (**2**)

1,1,2-Trimethylbenz[e]indolenine (2.09 g, 10 mmol) and 3-bromopropanesulfonic acid sodium salt (2.25 g, 10 mmol) were dissolved in NMP (20 mL). The solution was stirred for 84 h at 120 °C. After cooling to room temperature, the solution was added dropwise to 140 mL of acetone to precipitate the crude product. The suspension was centrifuged in 50 mL plastic tubes (5 min, 4500 rpm) and decanted. To every tube 35 mL of acetone was added and the pellets were resuspended to wash the product. Tubes were centrifuged again (5 min, 4500 rpm) and decanted. The product pellets were dried overnight in a desiccator yielding 3.22 g (7.41 mmol, 74%) of a purple/blue solid. MS: $[M + H]^+$ calculated 332.13, found 332.13.

2.2.2. 3-(2,3,3-trimethyl-3H-indol-1-ium-1-yl)propane-1-sulfonate (**3**)

1,1,2-Trimethylindolenine (1.0 g, 6.3 mmol) and 3-bromopropanesulfonic acid sodium salt (5.2 g, 18.9 mmol) were dissolved in NMP (10 mL). The solution was stirred for 48 h at 120 °C. After cooling to room temperature, the solution was added dropwise to 250 mL Et_2O/iPrOH (1:1 v/v) while stirring and the precipitated solids were collected by centrifugation in 50 mL plastic tubes (5 min, 3000 rpm) and decantation. The solids were redissolved in MeOH (20 mL) and re-precipitated from EtOAc (250 mL). After centrifugation, the product was washed with Et_2O and dried in a desiccator yielding 2.2 g (5.7 mmol, 90%) of a slightly pink solid. $[M + H]^+$ calculated 282.12, found 282.06; $[2M + H]^+$ calculated 563.22, found 563.24.

2.2.3. 1,2,3,3-tetramethyl-3H-indol-1-ium-5-sulfonate (**4**)

CH_3CN (60 mL) and iodomethane (6.23 mL, 100 mmol) were added to potassium 2,3,3-trimethyl-*3H*-indole-5-sulfonate (5.55 g, 20 mmol). The suspension was stirred overnight at 80 °C. After cooling to room temperature, the supernatant was decanted. MeOH (30 mL) and H_2O (3 mL) were added to dissolve the product. The obtained red solution was added dropwise to EtOAc (375 mL) while stirring. The obtained pink suspension was transferred into 50 mL plastic tubes, centrifuged (10 min, 3600 rpm) and decanted. To every tube 20 mL of EtOAc was added, the pellets were resuspended and combined in 4 50 mL tubes. The tubes were centrifuged (5 min, 4500 rpm) and decanted. To every tube 40 mL of Et_2O was added and the pellets were resuspended. Tubes were centrifuged (5 min, 4500 rpm) and decanted. The product was dried overnight in a desiccator yielding 7.16 g (17.1 mmol, 85%) of a pink solid. MS: $[M + H]^+$ calculated 254.09, found 254.04.

2.2.4. 2,3,3-trimethyl-1-(3-sulfonatopropyl)-3H-indol-1-ium-5-sulfonate (**5**)

Potassium 2,3,3-trimethyl-*3H*-indole-5-sulfonate (2.77 g, 10 mmol) and 3-bromopropanesulfonic acid sodium salt (2.25 g, 10 mmol) were dissolved in NMP (20 mL). The solution was stirred for 114 h at 120 °C. After cooling to room temperature, the supernatant was decanted from the precipitated solids and the residue was dissolved in MeOH (20 mL) and H_2O (10 mL). The solution was added dropwise to 600 mL of CH_3CN and the product precipitated. The suspension was filtered and the product was washed on the filter with CH_3CN. The product was dried overnight in a desiccator yielding 1.40 g (2.79 mmol, 28%) of a dark purple solid. MS: $[M + H]^+$ calculated 362.07, found 361.93.

2.2.5. 3-(2-((E)-2-((E)-2-chloro-3-((E)-2-(1,1-dimethyl-3-(3-sulfonatopropyl)-1,3-dihydro-2H-benzo[e]indol-2-ylidene)ethylidene)cyclohex-1-en-1-yl)vinyl)-1,1-dimethyl-1H-benzo[e]indol-3-ium-3-yl)propane-1-sulfonate (**6**)

Compound **2** (2.61 g, 6.0 mmol), compound **1** (1.08 g, 3.0 mmol) and sodium acetate (984 mg, 12 mmol) were dissolved in MeOH (60 mL). The mixture was refluxed for 3 h. After cooling of the mixture, 20 mL of MeOH was added and the mixture was added dropwise to 160 mL of Et_2O to precipitate the product. The suspension was filtered and the product was washed on the filter with 50 mL of Et_2O. The product was dried overnight in a desiccator yielding 2.19 g (2.74 mmol, 91%) of a brown/red solid. MS: $[M + H]^+$ calculated 799.26, found 799.26.

2.2.6. 3-((E)-2-((E)-2-(2-chloro-3-((E)-2-(3,3-dimethyl-1-(3-sulfonatopropyl)-3H-indol-1-ium-2-yl)vinyl)cyclohex-2-en-1-ylidene)ethylidene)-3,3-dimethylindolin-1-yl)propane-1-sulfonate (**7**)

Compound **3** (1.17 g, 3.0 mmol), compound **1** (500 mg, 1.4 mmol) and sodium acetate (0.37 g, 4.5 mmol) were dissolved in EtOH (20 mL). The mixture was refluxed for 16 h. After cooling to room temperature, the reaction mixture was precipitated by dropwise addition to EtOAc (500 mL). The solids were collection by filtration, redissolved in MeOH (25 mL) and precipitated from Et_2O/iPrOH 1:1 (v/v, 500 mL). The solids were collected by centrifugation and decantation, and after drying overnight the crude dye was obtained yielding 250 mg (0.34 mmol, 11%) of a black solid. MS: $[M + H]^+$ calculated 699.23, found 699.13; $[2M + H]^+$ calculated 1397.46,

found 1397.75; $[M + 2H]^{2+}$ calculated 350.12, found 350.29.

*2.2.7. 2-((E)-2-((E)-2-chloro-3-(2-((E)-1,3,3-trimethyl-5-sulfonatoindolin-2-ylidene)ethylidene)cyclohex-1-en-1-yl)vinyl)-1,3,3-trimethyl-3H-indol-1-ium-5-sulfonate (**8**)*

Compound **4** (99 mg, 0.24 mmol), compound **1** (42 mg, 0.118 mmol) and sodium acetate (29 mg, 0.354 mmol) were dissolved in EtOH (10 mL). The mixture was refluxed for 11 h. After cooling of the mixture, it was added dropwise to 80 mL of Et_2O to precipitate the product. The green suspension was centrifuged (5 min, 4500 rpm, 2 tubes) and decanted. To every tube 40 mL of Et_2O was added and the pellets were resuspended. Tubes were centrifuged (5 min, 4500 rpm) and decanted. The product was dried overnight in a desiccator yielding a black solid in quantitative yield. MS: $[M + H]^+$ calculated 643.17, found 643.17.

*2.2.8. 2-((E)-2-((E)-2-chloro-3-(2-((E)-3,3-dimethyl-5-sulfonato-1-(3-sulfonatopropyl)indolin-2-ylidene)ethylidene)cyclohex-1-en-1-yl)vinyl)-3,3-dimethyl-1-(3-sulfonatopropyl)-3H-indol-1-ium-5-sulfonate (**9**)*

Compound **5** (1.00 g, 2.0 mmol), compound **1** (359 mg, 1.0 mmol) and sodium acetate (246 mg, 3.0 mmol) were dissolved in EtOH (100 mL). The mixture was refluxed for 117 h. After cooling of the mixture, it was added dropwise to 400 mL of EtOAc to precipitate the product. The suspension was filtered and the product was washed on the filter with EtOAc. The product was dried overnight in a desiccator yielding a purple/blue solid in quantitative yield. MS: $[M + H]^+$ calculated 859.15, found 859.08.

*2.2.9. 3-(2-((E)-2-((E)-4′-(2-carboxyethyl)-6-((E)-2-(1,1-dimethyl-3-(3-sulfonatopropyl)-1,3-dihydro-2H-benzo[e]indol-2-ylidene) ethylidene)-3,4,5,6-tetrahydro-[1,1′-biphenyl]-2-yl)vinyl)-1,1-dimethyl-1H-benzo[e]indol-3-ium-3-yl)propane-1-sulfonate (**10**)*

Compound **6** (1.00 g, 1.25 mmol) and 4-(2-carboxyethyl)benzeneboronic acid (291 mg, 1.5 mmol) were dissolved in dioxane (20 mL) and H_2O (15 mL). Et_3N (700 μL, 5 mmol) was added and the solution was stirred under nitrogen. $Pd(PPh_3)_4$ (30 mg) was added under a nitrogen atmosphere and the mixture was stirred at 90 °C for 2.5 h. The solution was added dropwise to 160 mL of EtOAc/EtOH/formic acid (400:100:0.5) and the product precipitated. The suspension was centrifuged in 4 50 mL plastic tubes (5 min, 4500 rpm) and decanted. To every tube 30 mL of EtOAc/EtOH/formic acid (400:100:0.5) was added and the pellets were resuspended. Tubes were centrifuged (5 min, 4500 rpm) and decanted. To every tube 10 mL EtOH was added to dissolve the product and then 40 mL of EtOAc was added to each tube and the product precipitated. Tubes were centrifuged (5 min, 4500 rpm), decanted and the product was dried overnight in a desiccator yielding 570 mg (0.62 mmol, 50%) of a green solid.

The crude product (50 mg) was dissolved in DMSO (3 mL), H_2O/CH_3CN/TFA (75:25:0.1) (0.5 mL) and 1 M KCl (1 mL) to obtain potassium counterions of the sulfonate groups. The dissolved product was purified by preparative HPLC using a gradient of H_2O/CH_3CN/TFA 70:30:0.1 to H_2O/CH_3CN/TFA 50:50:0.1 in 28 min. After pooling and lyophilization of the appropriate fractions the product was obtained as a green fluffy solid. MS: $[M + H]^+$ calculated 913.36, found 913.23; $[M + 2H]^{2+}$ calculated 457.18, found 456.69.

HRMS: $[M - H]^-$ calculated 911.34053 for $C_{53}H_{55}N_2O_8S_2$, found 911.34117.

The dye (5.14 mg) was dissolved in 4 mM ethylene carbonate (internal standard for NMR) in DMSO-d6 (1350 μL) to afford a 4 mM solution, which was used for NMR and as a stock solution. ^{1}H NMR (DMSO-d6, 300 MHz) δ = 1.42 (s, 12H, 4 CH_3), 1.90–2.10 (m, 6H, 1 CH_2 cyclohexene, 2 $CH_2CH_2CH_2SO_3$), 2.56 (t, 4H, 2 $CH_2CH_2CH_2SO_3$), 2.76–2.80 (m, 4H, 2 CH_2 cyclohexene), 2.76–2.80 (m, 2H) and 3.10 (t, 2H) (CH_2CH_2COOH), 4.39 (t, 4H, 2 $CH_2CH_2CH_2SO_3$), 6.42 and 7.26 (2d, 2 × 2H, 2 × 2 vinylic CH), 7.21 and 7.54 (2 d, 2 × 2H, PhCH$_2$CH$_2$COOH), 7.44 (t, 2H), 7.58–7.63 (m, 2H), 7.76 (d, 2H), 7.99–8.03 (m, 4H) and 8.08 (d, 2H) (6 × CH benz[e]indolenine).

^{13}C NMR (DMSO-d6, 150 MHz) δ = 21.12, 23.59, 24.23, 25.44, 26.60, 30.37, 36.41, 40.06, 42.64, 47.84, 49.89, 99.92, 111.56, 122.12, 124.51, 127.45, 127.55, 128.64, 129.11, 129.83, 130.25, 131.16, 132.70, 136.49, 138.44, 139.85, 141.22, 146.50, 161.12, 172.43, 173.62.

*2.2.10. 3-((E)-2-((E)-2-(4′-(2-carboxyethyl)-6-((E)-2-(3,3-dimethyl-1-(3-sulfonatopropyl)-3H-indol-1-ium-2-yl)vinyl)-4,5-dihydro-[1,1′-biphenyl]-2(3H)-ylidene)ethylidene)-3,3-dimethylindolin-1-yl)propane-1-sulfonate (**11**)*

Compound **7** (82 mg, 0.12 mmol) and 4-(2-carboxyethyl)benzeneboronic acid (39 mg, 0.20 mmol) were dissolved in dioxane (2 mL) and H_2O (2 mL). Et_3N (84 μL, 0.60 mmol) was added and the solution was stirred under nitrogen. $Pd(PPh_3)_4$ (5 mg) was added under a nitrogen atmosphere and the mixture was stirred at 90 °C for 2.5 h. The solution was added dropwise to 40 mL of EtOAc/EtOH/formic acid (400:100:0.5) and the product precipitated. The suspension was centrifuged in a plastic tube (5 min, 4500 rpm) and decanted. The product was dried overnight in a desiccator yielding a green solid.

The crude product was dissolved in DMSO (1 mL), H_2O/CH_3CN/TFA (75:25:0.1) (0.5 mL), CH_3CN (0.5 mL) and 1 M KCl (2 mL) to obtain potassium counterions of the sulfonate groups. The dissolved product was purified by preparative HPLC using a gradient of H_2O/CH_3CN/TFA 80:20:0.1 to H_2O/CH_3CN/TFA 50:50:0.1 in 30 min. After pooling and lyophilization of the appropriate fractions the product was obtained as a green fluffy solid. MS: $[M + H]^+$ calculated 813.32, found 813.19; $[M + 2H]^{2+}$ calculated 407.17, found 406.75.

HRMS: $[M - H]^-$ calculated 811.30923 for $C_{45}H_{51}N_2O_8S_2$, found 811.31005.

The dye (4.76 mg) was dissolved in 4 mM ethylene carbonate (internal standard for NMR) in DMSO-d6 (1398 μL) to afford a 4 mM solution, which was used for NMR and as a stock solution.

^{1}H NMR (DMSO-d6, 300 MHz) δ = 1.10 (s, 12H, 4 CH_3), 1.94–1.98 (m, 6H, 1 CH_2 cyclohexene, 2 $CH_2CH_2CH_2SO_3$), 2.54 (t, 4H, 2 $CH_2CH_2CH_2SO_3$), 2.66–2.70 (m, 4H, 2 CH_2 cyclohexene), 2.66–2.70 (m, 2H) and 2.98 (t, 2H) (CH_2CH_2COOH), 4.25 (t, 4H, 2 $CH_2CH_2CH_2SO_3$), 6.37 and 7.11–7.17 (d and m, 2 × 2H, 2 × 2 vinylic CH), 7.11–7.17 and 7.31–7.49 (2m, 12H, Ar).

^{13}C NMR (DMSO-d6, 150 MHz) δ = 21.03, 23.31, 24.17, 27.09, 30.13, 35.71, 40.06, 42.45, 47.86, 48.13, 100.28, 110.96, 122.28, 124.35, 128.41, 128.55, 129.04, 131.10, 136.40, 140.69, 141.02, 142.18, 147.51, 161.65, 171.20, 173.50.

*2.2.11. 2-((E)-2-((E)-4′-(2-carboxyethyl)-6-(2-((E)-1,3,3-trimethyl-5-sulfonatoindolin-2-ylidene)ethylidene)-3,4,5,6-tetrahydro-[1,1′-biphenyl]-2-yl)vinyl)-1,3,3-trimethyl-3H-indol-1-ium-5-sulfonate (**12**)*

Compound **8** (97 mg, 0.15 mmol) and 4-(2-carboxyethyl)benzeneboronic acid (50 mg, 0.30 mmol) were dissolved in dioxane (2 mL) and H_2O (2 mL). Et_3N (146 μL, 1.05 mmol) was added and the solution was stirred under nitrogen. $Pd(PPh_3)_4$ (5 mg) was added under a nitrogen atmosphere and the mixture was stirred at 90 °C for 2.5 h. The solution was added dropwise to 80 mL of EtOAc/EtOH/formic acid (175:25:0.1) and the product precipitated. The suspension was centrifuged in 2 50 mL plastic tubes (5 min, 4500 rpm) and decanted. To every tube 5 mL EtOH was added to dissolve the product and then 20 mL of EtOAc was added to each tube and the product precipitated. Tubes were centrifuged (5 min, 4500 rpm), decanted and the product was dried overnight in a desiccator yielding 57 mg (0.075 mmol, 50%) of a brown solid.

The crude product (40 mg) was dissolved in H_2O/CH_3CN/TFA (75:25:0.1) (2 mL), CH_3CN (0.5 mL) and 1 M KCl (1 mL) to obtain potassium counterions of the sulfonate groups. The dissolved product was purified by preparative HPLC using a gradient of H_2O/CH_3CN/TFA 90:10:0.1 to H_2O/CH_3CN/TFA 60:40:0.1 in 30 min. After pooling and lyophilization of the appropriate fractions the product was obtained as a green fluffy solid. MS: $[M + H]^+$ calculated 757.26, found 757.39; $[M + 2H]^{2+}$ calculated 379.13, found 378.55.

HRMS: $[M - H]^-$ calculated 755.24663 for $C_{41}H_{43}N_2O_8S_2$, found 755.24735.

The dye (5.22 mg) was dissolved in 4 mM ethylene carbonate (internal standard for NMR) in DMSO-d6 (1643 μL) to afford a 4 mM solution, which was used for NMR and as a stock solution. ^{1}H NMR (DMSO-d6, 300 MHz) δ = 1.12 (s, 12H, 4 CH_3), 1.93 (t, 2H, CH_2 cyclohexene), 2.67–2.73 (m, 4H, 2 CH_2 cyclohexene), 2.67–2.73 (m, 2H) and 3.00 (t, 2H) (CH_2CH_2COOH), 3.56 (s, 6H, 2 CH_3), 6.16 and 7.14 (2d, 2 × 2H, 2 × 2 vinylic CH), 7.11, 7.25, 7.49 and 7.58 (4d, 8H, Ar), 7.62 (s, 2H, Ar).

^{13}C NMR (DMSO-d6, 150 MHz) δ = 20.93, 24.08, 26.87, 30.12, 31.19, 35.53, 40.06, 48.10, 100.49, 109.78, 119.68, 125.99, 128.60, 128.95, 130.87, 135.96, 139.92, 141.25, 142.79, 145.10, 146.95, 161.49, 171.98, 173.46.

2.2.12. 2-((E)-2-((E)-4′-(2-carboxyethyl)-6-(2-((E)-3,3-dimethyl-5-sulfonato-1-(3-sulfonatopropyl)indolin-2-ylidene)ethylidene)-3,4,5,6-tetrahydro-[1,1′-biphenyl]-2-yl)vinyl)-3,3-dimethyl-1-(3-sulfonatopropyl)-3H-indol-1-ium-5-sulfonate (**13**)

Compound **9** (430 mg, 0.50 mmol) and 4-(2-carboxyethyl)benzeneboronic acid (194 mg, 1.0 mmol) were dissolved in dioxane (6 mL) and H_2O (6 mL). Et_3N (627 μL, 4.5 mmol) was added and the solution was stirred under nitrogen. $Pd(PPh_3)_4$ (15 mg) was added under a nitrogen atmosphere and the mixture was stirred at 90 °C for 2.5 h. The solution was added dropwise to 80 mL of EtOAc/EtOH/formic acid (50:50:0.1) and the product precipitated. The suspension was centrifuged in 2 50 mL plastic tubes (5 min, 4500 rpm) and decanted. To every tube 20 mL EtOH was added to dissolve the product and then 20 mL of EtOAc was added to each tube and the product precipitated. Tubes were centrifuged (5 min, 4500 rpm), decanted and the product was dried overnight in a desiccator yielding 264 mg (0.27 mmol, 54%) of a green solid.

The crude product (40 mg) was dissolved in H_2O/CH_3CN/TFA (75:25:0.1) (2 mL), CH_3CN (0.5 mL) and 1 M KCl (1 mL) to obtain potassium counterions of the sulfonate groups. The dissolved product was purified by preparative HPLC using a gradient of 0.1% TFA in H_2O to H_2O/CH_3CN/TFA 70:30:0.1 in 30 min. After pooling and lyophilization of the appropriate fractions the product was obtained as a green fluffy solid. MS: $[M + H]^+$ calculated 973.24, found 973.30.

HRMS: $[M - 3H]^{3-}$ calculated 323.06944 for $C_{45}H_{49}N_2O_{14}S_4$, found 323.06959.

The dye (5.30 mg) was dissolved in 4 mM ethylene carbonate (internal standard for NMR) in DMSO-d6 (1218 μL) to afford a 4 mM solution, which was used for NMR and as a stock solution. ^{1}H NMR (DMSO-d6, 300 MHz) δ = 1.11 (s, 12H, 4 CH_3), 1.93–1.98 (m, 6H, 1 CH_2 cyclohexene, 2 $CH_2CH_2CH_2SO_3$), 2.56 (t, 4H, 2 $CH_2CH_2CH_2SO_3$), 2.68–2.72 (m, 4H, 2 CH_2 cyclohexene), 2.68–2.72 (m, 2H) and 3.00 (t, 2H) (CH_2CH_2COOH), 4.25 (t, 4H, 2 $CH_2CH_2CH_2SO_3$), 6.39 and 7.14 (2d, 2 × 2H, 2 × 2 vinylic CH), 7.14, 7.31, 7.47 and 7.56 (4d, 8H, Ar), 7.61 (s, 2H, Ar).

^{13}C NMR (DMSO-d6, 150 MHz) δ = 21.04, 23.16, 24.16, 27.02, 30.14, 35.58, 40.05, 42.57, 47.80, 48.14, 100.67, 109.90, 119.69, 126.01, 128.54, 128.96, 131.50, 136.16, 140.07, 141.11, 142.15, 144.83, 147.44, 161.80, 171.38, 173.47.

2.3. Spectrometry

2.3.1. Molar extinction coefficient and stacking behavior in different solvents

Absorption spectra of the dyes were measured on a Ultrospec 3000 (Amersham Pharmacia) using either 1 cm disposable plastic 1 mL cuvettes (Brand, Germany) for a concentration of <7 μM, 0.1 cm quartz cuvettes (Hellma standard cell, Macro) for higher concentrations (7–70 μM) or using two glass microscopy slides held together with a 0.14 mm thick PET plastic spacer for very high concentrations (>70 μM) to keep the signal below 1.5 AU. Stock solutions of **IRDye 800CW** were made according to its previously reported molar extinction coefficient (Table 2).

The stock solutions of the dyes in DMSO-d6 (see synthesis) were diluted down to 5 μM concentration in DMSO, water or phosphate buffered saline (PBS). A further twofold dilution range in same medium was made from this stock. The absorbance of the dyes at these concentrations was plotted and the linear regression coefficient was used for determination of the molar extinction coefficient (ε). The emission maximum was determined by measuring the emission spectrum of a 1 μM concentration of dye after excitation of the vibronic shoulder peak (around 720 nm, depending on the dye).

The stock solutions were diluted in DMSO, water or PBS at concentrations ranging from 1.25 μM to 125 μM and optical density was measured 10 min after preparation. The absorbance was plotted normalized for cuvette path length and concentration.

2.3.2. Quantum yield determination

Fluorescence spectra were obtained on a Perkin Elmer LS-55 equipped with a red-sensitive PMT using 1 cm square quartz cuvettes (Hellma). The absorption of the dyes at a concentration of 1 μM in DMSO at 720 nm was measured and after dilution, which was correlated with the integrated fluorescent emission after excitation at 720 nm. The regression coefficient of this plot of the unknown dyes **10**–**13** and **IRDye 800CW** was compared to the regression coefficient of **ICG**, of which the quantum yield was reported in literature [32].

2.3.3. Electron density modelling and log D calculations

Electrostatic potential mapping of the dyes was performed using Spartan'14 (Wavefunction, Irvine USA) using a semi-empirical model and the AM1 method on **ICG** and the methylamide form of dyes **IRDye 800CW** and **10**–**13** for comparison. The protonated form of the sulfonate groups was used to investigate the electron density on the cyanine backbone itself as the charged groups would otherwise dominate the electron potential energy around them. Log D was calculated using MarvinSketch (ChemAxon Kft Hungary).

2.4. Antibody labelling

2.4.1. Preparation of NHS esters of the dyes

IRDye 800CW-NHS was purchased from Licor. For the other dyes the following protocol was applied: Dye (0.17 μmol) and dipyrrolidino(N-succinimidyloxy)carbenium hexafluorophosphate (HSPyU, 0.51 μmol, 3 equiv) were dissolved in DMSO (50 μL) and 4-methylmorpholine (NMM, 2 μL) was added. After homogenisation, the mixture was allowed to stand for 30 min. The NHS esters were precipitated by adding the mixtures to EtOAc (1 mL). The suspensions were centrifuged (3 min, 10 000 g) after which the supernatant was discarded and the pellets were dissolved in DMSO (100 μL).

2.4.2. Labelling of trastuzumab

Trastuzumab (5 mg formulation (Herceptin) was used for each

Table 1
Net charge and lipophilicity as measured by cLog D of the dyes **ICG, 10–13** and **IRDye 800CW**.

Compound	Net charge of the free dye (and the $MeNH_2$ conjugate)	cLog D of the free dye at pH 7.4 (and the $MeNH_2$ conjugate)
ICG	−1 (n/a)	4.91 (n/a)
10	−2 (−1)	2.31 (5.35)
11	−2 (−1)	0.33 (3.37)
12	−2 (−1)	0.53 (3.58)
13	−4 (−3)	−6.06 (−3.02)
IRDye 800CW	−4 (−3)	−5.02 (−1.97)

Table 2
Photophysical properties of compounds **10–13** and reference compounds **ICG** and **IRDye 800CW**.

Dye	ε in DMSO[a] (M^{-1} cm^{-1})	ε in water[a] (M^{-1} cm^{-1})	ε in PBS[a] (M^{-1} cm^{-1})	$\lambda_{ex}/\lambda_{em}$ in DMSO (stokeshift) (nm)	$\lambda_{ex}/\lambda_{em}$ in H_2O and PBS (stokeshift) (nm)	Φ_F in DMSO
ICG	$1.95 \cdot 10^5$	$1.56 \cdot 10^5$	$0.88 \cdot 10^5$ [b]	794/821 (27)	780/802 (22)	12% [32]
10	$2.30 \cdot 10^5$	n.d.[c]	n.d.[c]	810/826 (16)	790/806[c] (16)	13%
11	$2.64 \cdot 10^5$	$1.52 \cdot 10^5$ [b]	$1.60 \cdot 10^5$ [b]	774/795 (21)	751/771 (20)	42%
12	$2.29 \cdot 10^5$	n.d.[c]	n.d.[c]	779/801 (22)	753/771 (18)	31%
13	$2.62 \cdot 10^5$	$2.44 \cdot 10^5$	$2.18 \cdot 10^5$	784/807 (23)	756/777 (21)	35%
IRDye 800CW	n/a[d]	$2.40 \cdot 10^5$ [35]	$2.40 \cdot 10^5$ [35]	796/818 (22)	775/806 (31)	21%

[a] Fresh dilutions from the DMSO stock were made and measured within 2 h.
[b] Significant non-linearity due to extensive dimerization, lower concentrations (<2 μM) were used for the calculation of the molar extinction coefficient instead.
[c] Concentration dependent intermolecular interactions could not be avoided even at the lowest measured concentrations.
[d] The molar extinction coefficient in this solvent was not available from literature, although it is expected to be similar to that of the compound in the other two solvents based on the relative values found in Table 2.

labelling, which contains approximately 2.5 mg of the antibody trastuzumab) was dissolved in H_2O (20 mg/mL), transferred to Amicon Ultra 100K centrifugal filters (500 μL in each filter device) and centrifuged until approximately 100 μL remained on the filters. 0.1 M HEPES (pH 8.5) was added (400 μL) and the filter devices were centrifuged to remove the excipients (2×). The antibody was recovered and aliquoted in portions of 2.5 mg trastuzumab (0.017 μmol) in 250 μL 0.1 M HEPES (pH 8.5) for each labelling.

Dye-NHS in DMSO (10 μL, 0.034 μmol) was added to the trastuzumab solution, after which the mixture was homogenized and incubated for 30 min. The unconjugated dye was removed using Amicon Ultra 100K centrifugal filters and 0.1 M HEPES (pH 7.2) (5×), yielding a solution of labelled trastuzumab in 250 μL 0.1 M HEPES (pH 7.2).

Absorption spectra were measured on a Ultrospec 3000 (Amersham Pharmacia) using 1 cm disposable plastic 1 mL cuvettes (Brand, Germany). The degree of labelling was calculated by normalizing the absorption spectra for antibody concentration as determined by the absorption at 280 nm. Next, the molar extinction coefficient in water was used for calculation of the ratio of absorbance at ~750 nm–280 nm. Stacked dyes were taken into account by calculating the area under the curve of the absorption spectra and comparing with the area of the curve of known concentrations of free dye in water at high dilution.

2.5. Chemical stability

2.5.1. Dye stability towards gluthathione

Nitrogen was bubbled through 0.1 M HEPES (pH 7.4) buffer to remove oxygen in an attempt to reduce the rate of disulfide-formation of glutathione. Subsequently, reduced glutathione was added to this buffer for a final concentration of 0.5 mM glutathione. Finally, 20 μL of dye stock solution in DMSO-d6 (see synthesis) was added to 300 μL of the glutathione solution, yielding a solution of 0.25 mM dye in 0.5 mM glutathione-containing buffer. This solution was immediately put into the sample manager (37 °C) of an UPLC-MS equipped with a Waters BEH C18 130 Å 1.7 μm (100 × 2.1 mm) column and using a gradient of 10 mM NH_4OAc/CH_3CN (95:5) to 10 mM NH_4OAc/CH_3CN (5:95) in 5.44 min. UPLC-MS analysis was performed every 30 min. The stability of the dyes was calculated relative to the integration of the chromatogram at t = 0.

2.5.2. Dye stability towards 5-aminovaleric acid

20 μL of dye stock solution in DMSO-d6 (see synthesis) was added to 300 μL of 20 mM 5-aminovaleric acid and 20 mM HEPES buffer (pH 7.4). This solution was immediately put into the sample manager (37 °C) of an UPLC-MS equipped with a Waters BEH C18 130 Å 1.7 μm (100 × 2.1 mm) column and using a gradient of 0.05% TFA in H_2O/0.04% TFA in CH_3CN 95:5 to 0.05% TFA in H_2O/0.04% TFA in CH_3CN 5:95 in 5.44 min for **10–12** and **ICG**, and a gradient of 0.05% TFA in H_2O/0.04% TFA in CH_3CN 95:5 to 0.05% TFA in H_2O/0.04% TFA in CH_3CN 60:40 in 13.44 min for **13** and **IRDye 800CW**. UPLC-MS analysis was performed at t = 0, 4, 8 h. The stability of the dyes was calculated relative to the integration of the chromatogram at t = 0.

2.6. Optical stability

1 μM solutions of dyes **10–13**, **ICG** and **IRDye 800CW** in aqueous DMSO (20% in 10 mM phosphate buffer pH 7.4) were transferred into 4.5 mL disposable plastic cuvettes (Kartell). These cuvettes were placed in front of the Hamamatsu PDE NIR-camera system and illuminated at maximum intensity for 30 min. At 5 min intervals the cuvettes were measured by a PerkinElmer LS 55 spectrofluorometer equipped with a red-sensitive PMT with excitation at 720 nm.

3. Results and discussion

3.1. Design and synthesis

All four negatively charged NIR dyes were prepared by condensation of dianiline **1** with different alkylated indoles (**2–5**:

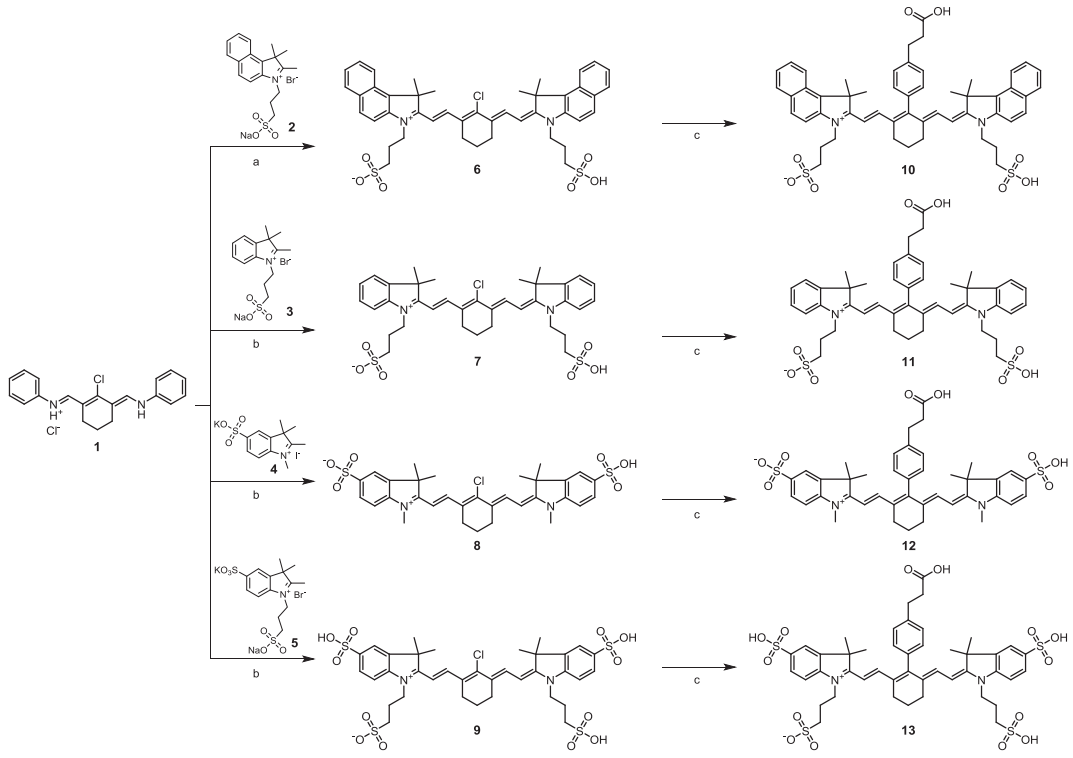

Scheme 1. Synthesis of compounds **10**–**13**. Legend: a) **2**, NaOAc, MeOH, reflux, b) **3**–**5**, NaOAc, EtOH, reflux, c) 4-(2-carboxyethyl)benzeneboronic acid, $Pd(PPh_3)_4$, Et_3N, dioxane/water, 90 °C.

Scheme 1). The obtained intermediates **6**–**9** all contained a chlorine atom, which was replaced by a 3-phenylpropanoic acid moiety by means of a Suzuki coupling using 4-(2-carboxyethyl)benzeneboronic acid, yielding stable C–C bonds [29]. 4-(2-Carboxyethyl)benzeneboronic acid was used instead of 4-carboxyphenylboronic acid, because aliphatic carboxylic acids are more reactive than aromatic carboxylic acids, a feature that facilitates the later conjugation of the dye with proteins and peptides in subsequent applications. The incorporation of the extra ethylene moiety did not result in significantly different photophysical properties in a zwitterionic C–C bonded dye previously reported by different groups [24,25].

Dye **10** was prepared to generate a symmetrical "ICG-like" dye that is suitable for conjugation. During the design, replacement of the benzoindolenine rings with the smaller indolenine rings in dye **11** was envisioned to decrease Van der Waal's forces between the reduced aromatic flat surface of the dye, which should in turn reduce the degree of dye–dye interactions. Dye **12** differs from dye **11** in the location of the sulfonate groups. Here, ring-sulfonation was introduced, as this feature is reported to reduce dye–dye interaction due to coulombic repulsion near the rings [33]. Dye **13** has sulfonate moieties on the aromatic rings as well as on the alkyl chains, creating the highest charge density, which should lead to dye–dye repulsion and thus decreased amounts of stacking.

3.2. Chemical properties

In Table 1, the net charge and cLog D values are provided for the compounds evaluated. Parent compound **ICG** and the structurally related compound **10** have similar lipophilic benzoindolenine rings, but **10** has a substantially lower cLog D due to its charged carboxylic acid (see Table 1). Substitution of the benzoindolenine building blocks for indolenine building blocks in compound **11** reduced the cLog D of the molecule while keeping the net charge equal. Moving the charged sulfonate groups from the alkyl chains to the aromatic rings as seen in compound **11** and **12** only had a minor effect on the cLog D. Finally, incorporating two additional charged sulfonate groups in **13** led to a substantially reduced cLog D, which was in line with the values found for **IRDye 800CW**. It should be noted that the clog D values of all carboxylic acid-containing dyes are increased upon conjugation with an amine as happens during a conjugation reaction, such as the simple amine $MeNH_2$ used as example (see Table 1).

In an attempt to visually present the difference in electron distribution between the dyes, we generated electrostatic potential maps using Spartan modelling software. The sulfonate moieties of the dyes were protonated to allow for modelling and comparison between dyes with the same net charge. Despite this limitation, Fig. 3 nicely illustrates that the structural modifications made clearly effects the electron density in the aromatic planes, a feature that could be critical for the stacking behavior of the dyes.

3.3. Photophysical properties

The molar extinction coefficients of dyes **10**–**13** and **ICG** were determined in water, PBS and DMSO, a highly polar aprotic solvent. To avoid concentration-dependent effects, dilution ranges of the dyes were measured and the linear (dilute) concentrations were used to calculate the molar extinction coefficient via the regression coefficient between concentration and absorbance (Table 2). In DMSO all dyes possessed high molar extinction coefficients. The molar extinction coefficient of **ICG** was measured at $1.95 \cdot 10^5\ M^{-1}\ cm^{-1}$, which shows good correlation with the reference value for **ICG** in 2:1 v/v CH_3CN/DMSO ($2.00 \cdot 10^5$) [34]. Dyes **10**–**13** showed somewhat higher molar extinction coefficients ranging from $2.29 \cdot 10^5$ to $2.64 \cdot 10^5\ M^{-1}\ cm^{-1}$.

In water the molar extinction coefficient was overall lower than

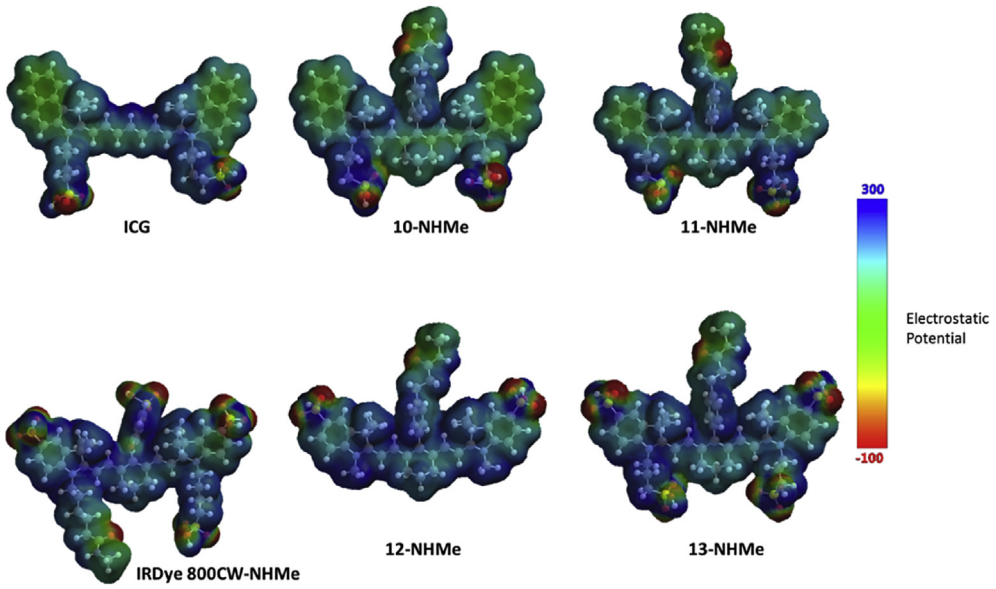

Fig. 3. Electrostatic potential map of the dyes **ICG,** the methylamides of dyes **10**–**13** and **IRDye 800CW** overlaid over ball-and-stick models. A higher electron density is repulsive to negative charges and depicted in red colors while a lower electron density, attractive to negative charges, is depicted in blue colors. (For interpretation of the references to color in this figure legend, the reader is referred to the web version of this article.)

that measured in DMSO, with the most hydrophilic dyes, **13** and **IRDye 800CW** showing very little reduction in molar extinction coefficient ($2.18 \cdot 10^5$ M^{-1} cm^{-1} for **13** and $2.4 \cdot 10^5$ M^{-1} cm^{-1} for **IRDye 800CW**). In contrast, Dyes **11** and **12** showed around 40% reduction in molar extinction coefficient when measured in water compared with DMSO decreasing to $1.52 \cdot 10^5$ M^{-1} cm^{-1} for **11**. The molar extinction coefficient of **12** could not be accurately determined due to occurrence of a small amount of stacking even at the lowest concentration measured, but was similar to that of **11**. Similarly, **ICG** showed a decrease in molar extinction coefficient down to $1.56 \cdot 10^5$ M^{-1} cm^{-1}. The molar extinction coefficient of dye **10** could not be calculated due to extensive stacking at all concentrations measured.

Changing the solvent to PBS did not affect the molar extinction coefficient of dyes **11**–**13** nor **IRDye 800CW** significantly (Table 2). For **ICG**, a further drop in the molar extinction coefficient yielded $0.88 \cdot 10^5$ M^{-1} cm^{-1}.

The absorption and emission peaks of the compounds (see Table 2), especially in water, varied between dyes. **ICG**, **10** and the aryl ether-containing dye **IRDye 800CW** displayed more red-shifted spectral properties in relation to compounds **11**–**13**. In **ICG** and compound **10**, the benzoindolenine moieties are responsible for a red shift compared with compounds lacking this double ring system. Likewise, the aryl ether moiety in **IRDye 800CW** causes a redshift in the absorption and emission spectra. Conjugation of all dyes to an antibody causes a modest redshift (vide infra) of around 2 nm. Although not relevant to the chemical properties, the position of the absorbance- and fluorescence maxima of these near infrared dyes dictate their compatibility with clinical camera systems, which generally are optimized for ICG detection.

For comparative reasons, quantum yields were determined in DMSO. It should be noted, however, that in water or PBS these values will be substantially lower, a feature that was previously reported for e.g. **ICG** [32]. The quantum yields of the dyes **11**–**13** ranged from 31% to 42% in DMSO, indicating superior quantum yield to the reference compound **ICG** (12%) and slightly higher than the ether-containing dye **IRDye 800CW** (21%). Dye **13** in particular combines a relatively high molar extinction coefficient (see above), both in DMSO and in aqueous systems, with a relatively high quantum yield. The quantum yield of compound **10** was nearly identical to that of **ICG** and amongst the lowest of the dyes tested, suggesting the presence of the benzoindolenine moiety has a negative effect on the quantum yield.

3.4. Dye stacking

The stacking behavior of the dyes was studied at concentrations ranging from 0.6 μM to 125 μM and in three solvents: DMSO, water and PBS (see Fig. 4 for the corresponding absorption spectra).

In DMSO, the absorption spectrum of all dyes tested was concentration independent. From this it is inferred that stacking is prevented as the dye molecules are all fully solvated by DMSO; a polar aprotic solvent that has the ability to solvate both charged groups as well as hydrophobic parts of the molecule. On the other hand, a concentration-dependent absorption spectrum was observed in water for dyes **10**–**13** and **ICG**. Different from DMSO, water is unable to effectively solvate the relatively flat and hydrophobic core of the cyanine dyes, which results in dye–dye stacking through Van der Waal's force at higher concentrations (see Fig. 1).

The absorbance of **ICG** remained relatively unaffected by concentrations up to 5 μM. Higher than that, a second peak indicative for dimer formation became apparent [10]. At a concentration of 125 μM, this dimer peak was the dominant peak. For the related dye **10**, concentration-dependent effects were also observed. Even at the lowest concentrations tested (0.3 μM and 0.6 μM) dimer peaks can readily be observed. At concentrations of 2.5 μM and higher, higher aggregation states of the dye in solution became visible as a blue-shifted (broader) shoulder peak. This indicates an increased propensity of dye **10** to form higher order structures in water in comparison with **ICG**. This trend can be explained by the surface area of the relatively planar and rigid core of the molecules, which is larger in dye **10** than it is in **ICG** and contributes to a greater Van der Waal's force (see Table 1 and Fig. 3). This trend is further illustrated by the cLog D of these compounds (see Table 1).

Dye **11** and **12** also show a high propensity to form dimers, even at the lowest concentrations of 0.3 μM and 0.6 μM, albeit to a lower

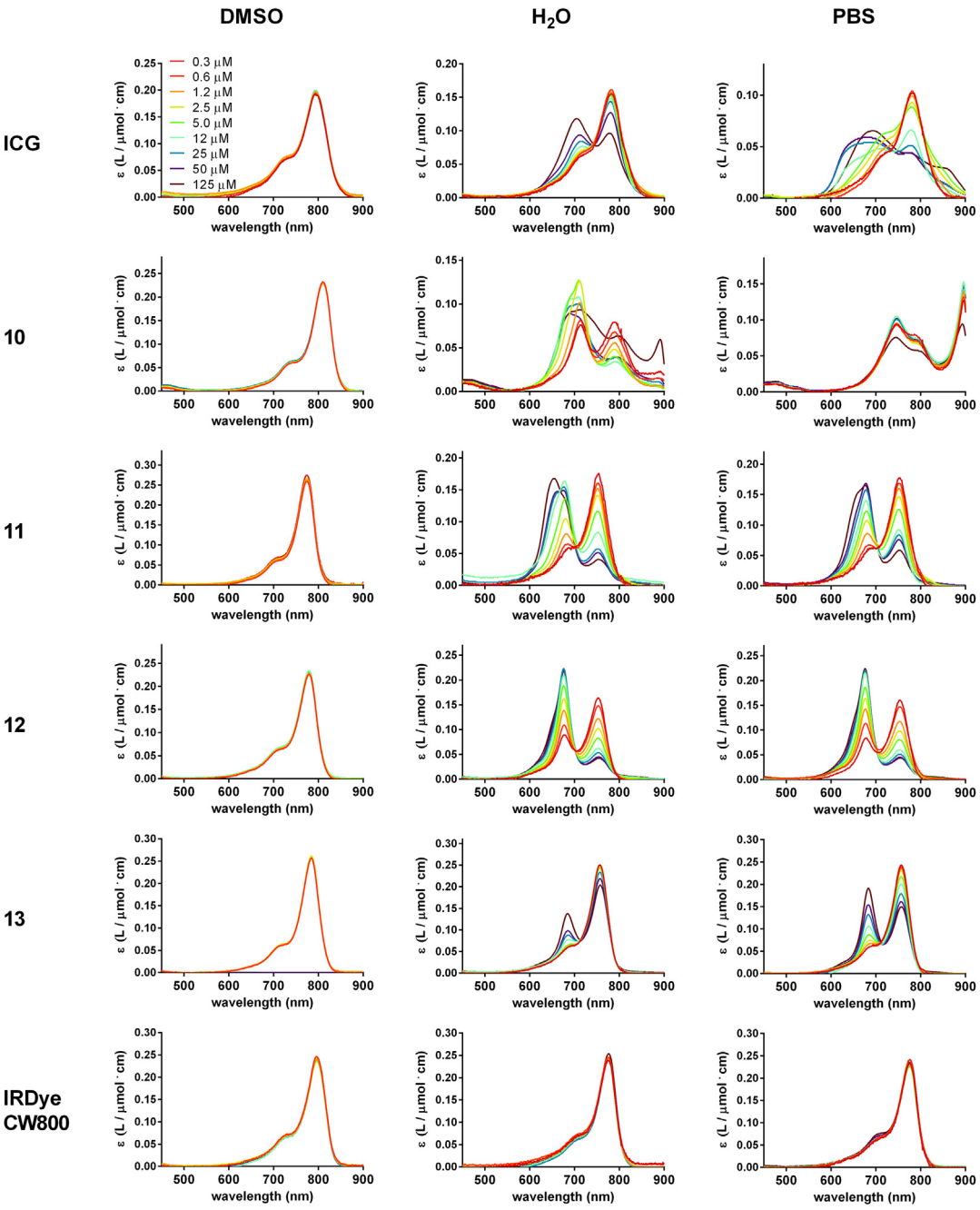

Fig. 4. Absorbance spectra of compounds **ICG**, **10**–**13** and **IRDye 800CW** in DMSO (left column), water (middle column) and PBS (right column).

extent than **10**. Interestingly, dye **12** forms higher order (H-type) structure less readily than **11**, with only a small amount of oligomeric dye aggregates observed in solution at the highest concentrations tested. The difference between compound **11** and **12**, which have a similar clog D value, is a direct result of the location of the negatively charged sulfonate group within the dye; Dye **11** has a relatively flexible alkyl tail that terminates in the sulfonate group and can accommodate the formation of a dimer and higher oligomers with as little as possible charge repulsion. Compound **12**, in contrast, lacks this flexibility thus accommodating the formation of dimers, but limiting the freedom to form higher-order aggregates.

The most negatively charged dye **13**, in line with expectations that increased charge repulsion leads to lower dye–dye interactions [33], is relatively unaffected by concentration-dependent effects in water; only at concentrations higher than 10 μM a small amount of dimerization becomes apparent. **IRDye 800CW** did not show any concentration dependence under these conditions.

PBS buffer contains ions, which can shield charges on the dye and can increase the polarity of the bulk solvent. Overall the concentration-dependent effects on the absorption spectra were similar or slightly stronger compared to those observed in pure water. There were two notable exceptions: **ICG** already formed dimers at a concentration of 0.6 μM in PBS, an order of magnitude difference compared with observations made in water. Above 5 μM, higher order aggregates were formed that included structures with red shifted absorption peaks (J-aggregates). Compound **10** displayed an even more extensive dye aggregation, including defined large J-aggregates recognizable by their sharp absorption band

similar to **ICG**. This aggregation was readily observed by the naked eye as dark green precipitate was formed. This suggest that the increased dye–dye interactions measured in PBS of **ICG** and **10** are caused predominantly by their benzoindolenine moieties.

3.5. Dye stacking during protein labelling

The ultimate application of the NIR dyes evaluated in this study would be their conjugation to a protein such as a monoclonal antibody. In such a conjugate they can provide an effective imaging agent for fluorescence-guided surgery. To this end, the effect of dye stacking on the conjugation efficacy and the photophysical properties of the conjugates had to be evaluated. To provide a proof-of-concept, the (therapeutic) antibody Trastuzumab, which is clinically used to target the HER2 receptor, was labelled with the NIR dyes. Trastuzumab was functionalized with all amine-reactive dyes. To reduce dye solubility problems labelling was performed at a relatively low concentration (~125 μM) and 2:1 ratio dye: antibody. Following purification, the resulting conjugates were diluted to 2.5 μM in HEPES buffer and the absorbance spectra were measured (Fig. 5B). The distribution between the stacked and "free" dye component on the conjugates represented by the absorption spectra generally corresponds to the absorbance spectra of the unconjugated dyes at concentration matching the labelling conditions (Fig. 5A, based on data from Fig. 4). This comparative data indicates the aggregation state of a dye during labelling conditions dictates the degree of stacking that is observed in the conjugate.

Stacking behavior of dyes on conjugates has also been described by Pauli et al. who suggest that dye-dimers may couple to proteins in addition to monomeric dye [18]. Additionally it was reported by the same authors that addition of BSA proved ineffective in reducing dye–dye interactions on antibodies, while complete protein unfolding by SDS on the other hand, did increase fluorescence and decrease stacking. This second experiment, which is based on the geometric rearrangement of the protein, indicates that two (or more) stacked dyes were conjugated in close proximity to each other [18].

The non-fluorescent stacked dyes in a conjugate may influence its properties; dyes are relatively large and charged, which in term may effect biodistribution. Therefore, dyes that do not contribute to the overall fluorescence are undesirable for imaging applications. Dye **10** showed a vast amount of stacking in the conjugate. In fact, stacking interactions were so strong that during labelling a large part of the NHS ester of dye **10** precipitated, severely limiting the labelling ratio and the amount of recovered conjugate. Thus, dye **10** was found unsuitable for dye conjugation using this setup. Dye **11** and **12** also demonstrated extensive stacking when conjugated to the antibody similar to the stacking behavior of the free dyes at 125 μM. Compound **13** only slightly stacked on trastuzumab while **IRDye 800CW** showed practically no stacking under these conditions.

When the degree of labelling of an antibody is determined by only measuring the absorbance at 280 nm (λ_{max} antibody) and at the λ_{max} of the dye, which is often the case, stacked dyes are unintentionally ignored, leading to a significant underestimation of the degree of labelling of the antibody (the amount of dyes per antibody). This may underestimate the effect that the dye has on the overall properties. This will be especially prominent when smaller targeting proteins such as nanobodies are functionalized [23]. When the calculation is based by the area under the curve, the degree of labelling was found to be 1.5 for **11** and **12** while it would be calculated 0.5 by the λ_{max} alone. For **13** this difference was less prominent and changed from 0.7 to 0.9. The labelling ratio for **IRDye 800CW** was found to be 1.1, which was independent of the way the calculation was performed. The degree of labelling was very similar for the various activated OSu-esters tested.

3.6. Chemical stability

To assess the in vivo stability of the dyes, all dyes were incubated at 37 °C in model buffers containing either glutathione or 5-aminovaleric acid to mimic endogenous nucleophiles and the solutions were analyzed over time by UPLC-MS based on the setup described by Nani et al. used for the analysis of chemical stability of aryl ether dyes [26]. A concentration of 0.5 mM of glutathione was used, as this is comparable to the concentration of free thiol as measured in healthy human serum [36]. For 5-aminovaleric acid a concentration of 20 mM was chosen to represent endogenous lysine side-chains. While optical spectroscopy can easily distinguish the intact dye from the 5-aminovaleric acid adduct, the glutathione adduct is far harder to distinguish from the parental dye by optical methods due to their similarity in photophysical properties [28]. In contrast, the dye and both adducts can be easily discriminated with UPLC-MS, thus providing a more accurate readout.

Dyes **10**–**13** and **ICG** were found to be fully stable towards both 5-aminovaleric acid and glutathione within a 8 and 6 h timeframe, respectively (Fig. 6A and C), similar to what was reported earlier for the **ZW800-1C** analogue based on the same dye core [25]. Longer incubation times led to significant (air) oxidation of glutathione that could be substantially reduced, but not eliminated, by purging the samples with nitrogen gas prior to incubation preventing accurate assessment of dye stability over longer time frames.

As stated above, aryl ether-containing NIR dyes like **ZW800-1**

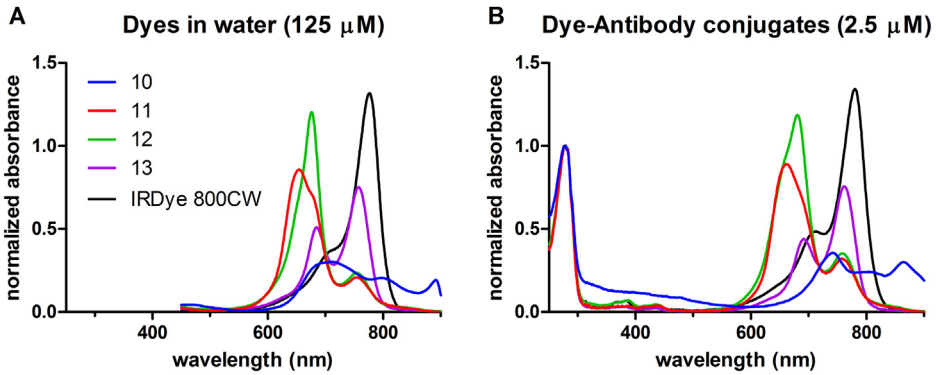

Fig. 5. A) Absorbance spectra of **10**–**13** and **IRDye 800CW** at 125 μM in water (data from Fig. 4 with absorbance normalized to match the λ_{max} of Fig. 5B). B) Absorbance spectra of the respective purified Trastuzumab-conjugates at approximately 2.5 μM with absorbance normalized to antibody absorbance at 280 nm.

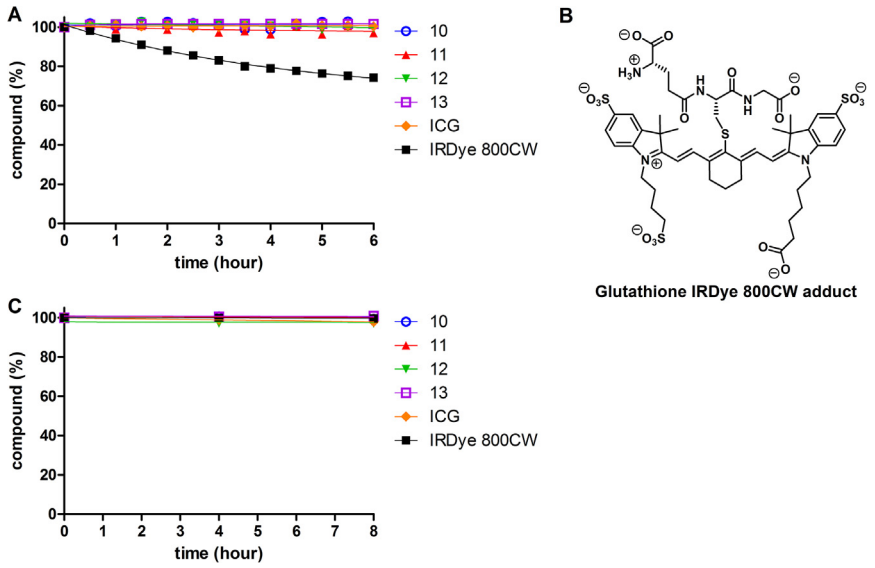

Fig. 6. Chemical stability: A) Dye stability in 0.5 mM glutathione in 0.1 M HEPES (pH 7.4) at 37 °C as assayed by UPLC-MS, B) Structure of the side product as a result of nucleophilic substitution on **IRDye 800CW** occurring by glutathione C) Dye stability in 20 mM 5-aminovaleric acid in 20 mM HEPES (pH 7.4) at 37 °C as assayed by UPLC-MS (see also Supplementary Information).

are reported to be unstable towards nucleophiles (amines and thiols) whereby the ether bond is cleaved upon nucleophilic attack [20,25,26]. Nucleophilic attack of an amine moiety gives rise to a compound with distinctly different photophysical properties from both the thiol adduct and the parent dye, which is also visible by the naked eye by a change in color towards blue [28]. In contrast, attack by a thiol moiety keeps the fluorescence properties of the dye intact [28].

An important distinction to be made is the position of the carboxylic acid functionality of the dye that is used for subsequent conjugation to targeting molecules. In symmetrical aryl ether-containing dyes, e.g. **ZW800-1**, the carboxylic acid is located on the aryl ether. In this case nucleophilic attack causes cleavage of the carboxylic acid functionality (that is used for conjugation) from the dye (Table 3). In contrast, in asymmetrical dyes, e.g. **IRdye 800CW** cleavage of the same bond will not result in loss of the carboxylic acid due to the different position of this moiety, despite elimination of the phenol moiety and addition of the (thiol-)nucleophile to the dye (Table 3).

In contrast to dyes **10**–**13** and **ICG**, **IRDye 800CW** was found to be susceptible to chemical degradation by thiols similar to other reported aryl ether containing cyanine dyes [24–27] (Fig. 6). The glutathione adduct with concomitant release of 4-hydroxybenzenesulfonate accounted for 26% of the dye after 6 h, a similar percentage compared with the stacked dye on antibody labelled with **13**. Depending on the structure of the thiol, which could be a

Table 3
Schematic overview of the differences between the ideal singular dye-labelling of antibodies and, respectively, a higher degree of dye labelling, nucleophile-dye adducts on antibody conjugates and nucleophile-mediated cleavage of the dye from the antibody.

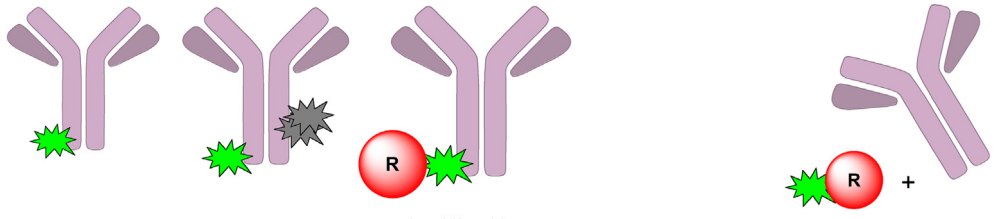

	Single dye on antibody	Multiple (stacked) dyes on antibody	Nucleophile adduct on asymmetric dye-antibody conjugate	Nucleophile adduct on symmetric dye-antibody conjugate, cleaved from antibody
Affinity of fluorescent construct for targeted receptor	Optimal	Possibly reduced [22]	Likely reduced, dependent on size and nature of R[a]	No affinity for original target [24,25]
Bio-distribution	Optimal [5]	Possibly altered [22]	Likely altered, strongly dependent on size and nature of R[a]	Altered, dictated by the size and nature of R[a]
Fluorescence intensity	Optimal	Reduced	Intact [28]	Intact if R is a thiol and reduced if R is an primary amine [28]
Chance of false positives[b]	Minimal	Increased possibility	Increased possibility, dependent on the nature of R[a] and the potential affinity for (other) targets of R[a]	High, fully defined by the nature of R[a] and potential affinity for (other) targets of R[a]

[a] R can in theory be any accessible endogenous nucleophile such as a thiol or amine, varying from small molecules to full length proteins.
[b] During image guided surgery, the fluorescence signal is assumed to correspond to the location of the targeted receptor. Fluorescence that does not correspond with the target risks misidentification of normal tissue as tissue containing the targeted biomarker.

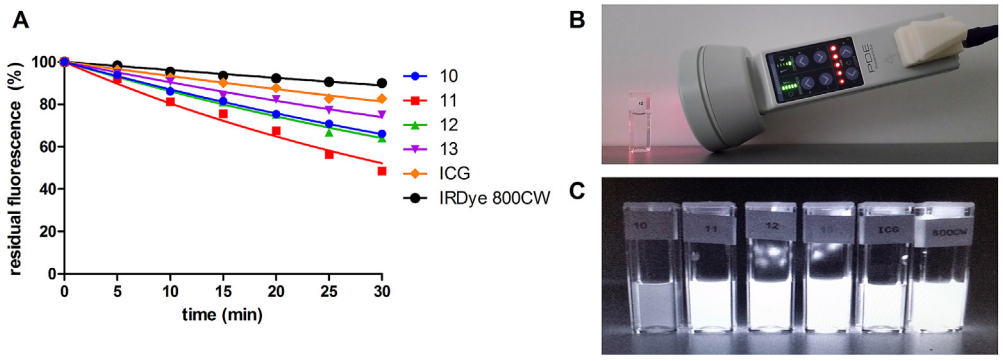

Fig. 7. A) Time-dependent optical stability of dyes **10**–**13**, **ICG** and **IRdye 800CW** upon illumination with the clinical grade Hamamatsu PDE camera system. B) The Hamamatsu PDE camera system illuminating the cuvette. C) Observation of fluorescence by the PDE camera system during the illumination process.

relatively small molecule like glutathione but in theory also large cysteine-containing proteins like albumin, a new structure is formed that may behave markedly different in vivo from its parental structure. Amine-related degradation products of **IRDye 800CW** were not observed by us, suggesting a greater stability towards amine nucleophiles than towards thiols.

When applied in surgical guidance, surgeons are expected to remove the fluorescent tissue from the patient. As such, the (time dependent) stability of dyes is of influence on their clinical use; conjugated to an antibody, a dye may reside in vivo for 48 h prior to its use in the operating room [37,38]. Thiol adducts such as those formed *in vitro* by **IRDye 800CW** possess similar absorbance and fluorescence properties to the antibody-dye conjugate and, therefore, may confound analysis (see Table 3).

3.7. Optical stability

To assess the optical stability of the dyes under conditions that are used for intra-operative imaging, dilute samples of the dyes in aqueous buffer were placed under the light source of the clinical grade Hamamatsu PDE NIR-fluorescence camera system (Fig. 7A and B) [15]. The samples were exposed to the light source with exclusion of ambient light for up to 30 min with assessment of the fluorescence signal. This timeframe is much longer than the typical 5–10 min fluorescence imaging time needed for the resection of one lymph node [15,39]. The fluorescence of all dyes was clearly visible with the PDE camera (Fig. 7C).

Dyes **10**–**13** showed increased photobleaching compared to **ICG** with subtle differences in the rate of bleaching between the different dyes. The least photo stable dye **11** showed a two-fold higher rate of bleaching (50% remaining fluorescence after 30 min) than the most stable dye of the set **13** (75% remaining), that approached **ICG** in stability (80%). Please note that photobleaching of **ICG** is not observed in the ongoing clinical trials running within our group (currently > 750 patients included in studies) [15,39].

4. Conclusion

Due to the excellent photophysical properties of both the aryl ether dyes and C–C bond containing dyes, the choice of NIR dye for protein labelling at the moment is based on the toleration of the negative features of the dye. The C–C bond-containing NIR dyes synthesized in this report (**10**–**13**) are synthetically easily accessible, possess improved photophysical properties compared to the clinically approved dye **ICG**, and seem to be fully stable towards hydrolysis, aminolysis and thiolysis for at least 6 h. However, in aqueous solutions, the C–C bond seems to enhance the tendency to form non-fluorescent dye-aggregates. Hereby, the degree of stacking observed for the free dyes at labelling concentrations, seems to be representative for the stacking observed for the dye-antibody conjugates. When stacking occurs in conjugates, for example the 30% as observed for **13**, it may: lead to an underestimation of the actual dye-functionalization rate, decrease the fluorescence intensity, and influence biodistribution in vivo to a small extent. However, the product can be purified and analyzed in detail. Introduction of charged (sulfonate groups) seems to counteract the stacking process, while the introduction of aromatic groups enhances it. The sulfonated aryl ether-containing NIR dye that is commonly used (**IRdye 800CW**) is far less prone to stacking, which facilitates mono-functionalization of antibodies. However, this reduced tendency to stack seems to be offset by its *in vitro* instability towards endogenous nucleophiles e.g. the 26% of **IRdye 800CW**-thiol adduct observed. It is currently, however, not clear to which extent such side products are formed in vivo, what type of side products occur in vivo, and if there are external factors that may influence this process. In our view both dye-stacking and dye-instability should be avoided and thus further synthetic efforts are required in order to provide an optimal NIR-dye for in vivo use.

Acknowledgments

We gratefully acknowledge the funding from the European Research Council under the European Union's Seventh Framework Program (FP7/2007-2013) and in particular ERC grant 2012-306890 and ERC grant 2012-323105, in addition to the Dutch VIDI grant of the Organization for Scientific Research (STW BGT 11272) and a Dutch Cancer Society translational research award (grant PGF 2009-4344). Furthermore, Anton Bunschoten (Wageningen University) is gratefully acknowledged for measuring ^{13}C NMR and Marcus T. M. Rood is gratefully acknowledged for helpful discussions on photophysical property determination of cyanine dyes.

Appendix A. Supplementary data

Supplementary data related to this article can be found at http://dx.doi.org/10.1016/j.dyepig.2016.03.054.

References

[1] van Leeuwen FWB, Hardwick JCH, van Erkel AR. Radiology 2015;276:12–29.
[2] Chin PTK, Beekman CAC, Buckle T, Josephson L, Van Leeuwen FWB. Am J Nucl Med Mol Imaging 2012;2:151–62.
[3] Burggraaf J, Kamerling IMC, Gordon PB, Schrier L, de Kam ML, Kales AJ, et al. Nat Med 2015;21:955–61.
[4] Luo S, Zhang E, Su Y, Cheng T, Shi C. Biomaterials 2011;32:7127–38.
[5] Zhou Y, Kim Y-S, Milenic DE, Baidoo KE, Brechbiel MW. Bioconjug Chem

2014;25:1801–10.
[6] Lavis LD, Raines RT. ACS Chem Biol 2008;3:142–55.
[7] Landsman ML, Kwant G, Mook GA, Zijlstra WG. J Appl Physiol 1976;40:575–83.
[8] Wang M, Silva GL, Armitage BA. J Am Chem Soc 2000;122:9977–86.
[9] Maskasky JE. Langmuir 1991;7:407–21.
[10] West W, Pearce S. J Phys Chem 1965;566:1894–903.
[11] Yao H, Domoto K, Isohashi T, Kimura K. Langmuir 2005;21:1067–73.
[12] Moody ED, Viskari PJ, Colyer CL. J Chromatogr B Biomed Sci Appl 1999;729:55–64.
[13] Buckle T, van Leeuwen AC, Chin PTK, Janssen H, Muller SH, Jonkers J, et al. Nanotechnology 2010;21:355101.
[14] KleinJan GH, van den Berg NS, Brouwer OR, de Jong J, Acar C, Wit EM, et al. Eur Urol 2014;66:991–8.
[15] van den Berg NS, Brouwer OR, Schaafsma BE, Matheron HM, Klop WMC, Balm AJM, et al. Radiology 2015;275:521–9.
[16] Choi HS, Nasr K, Alyabyev S, Feith D, Lee JH, Kim SH, et al. Angew Chem Int Ed 2011;50:6258–63.
[17] Pescitelli G, Di Bari L, Berova N. Chem Soc Rev 2014;43:5211.
[18] Pauli J, Grabolle M, Brehm R, Spieles M, Hamann FM, Wenzel M, et al. Bioconjug Chem 2011;22:1298–308.
[19] Mujumdar SR, Mujumdar RB, Grant CM, Waggoner AS. Bioconjug Chem 1996;7:356–62.
[20] Zhegalova NG, He S, Zhou H, Kim DM, Berezin MY. Contrast Media Mol Imaging 2014;9:355–62.
[21] Shibata M, Ihara H, Hirayama C. Polymer (Guildf) 1993;34:1106–8.
[22] Cohen R, Stammes MA, de Roos IHC, Stigter-van Walsum M, Visser GWM, van Dongen GAMS. EJNMMI Res 2011;1:31.
[23] Muyldermans S. Annu Rev Biochem 2013;82:775–97.
[24] Su D, Teoh CL, Samanta A, Kang N-Y, Park S-J, Chang Y-T. Chem Commun 2015;51:3989–92.
[25] Hyun H, Owens EA, Narayana L, Wada H, Gravier J, Bao K, et al. RSC Adv 2014;4:58762–8.
[26] Nani RR, Shaum JB, Gorka AP, Schnermann MJ. Org Lett 2015;17:302–5.
[27] Lim SY, Hong KH, Il Kim D, Kwon H, Kim HJ. J Am Chem Soc 2014;136:7018–25.
[28] Njiojob CN, Owens EA, Narayana L, Hyun H, Choi HS, Henary M. J Med Chem 2015;58:2845–54.
[29] Lee H, Mason JC, Achilefu S. J Org Chem 2006;71:7862–5.
[30] Berezin MY, Lee H, Akers W, Achilefu S. Biophys J 2007;93:2892–9.
[31] Hyun H, Bordo MW, Nasr K, Feith D, Lee JH, Kim SH, et al. Contrast Media Mol Imaging 2012;7:516–24.
[32] Benson RC, Kues HA. Phys Med Biol 1978;23:159–63.
[33] Mujumdar RB, Ernst LA, Mujumdar SR, Lewis CJ, Waggoner AS. Bioconjug Chem 1993;4:105–11.
[34] Kwon Lee S, Bard AJ. Anal Lett 1998;31:2209–29.
[35] LI-COR Biosciences, IRDye 800CW NHS Ester infrared dye product sheet, 2007.
[36] da Costa CM, dos Santos RCC, Lima ES, Bras J. Patol Med Lab 2006;42:345–50.
[37] Sampath L, Kwon S, Ke S, Wang W, Schiff R, Mawad ME, et al. J Nucl Med 2007;48:1501–10.
[38] Dijkers EC, Oude Munnink TH, Kosterink JG, Brouwers AH, Jager PL, de Jong JR, et al. Clin Pharmacol Ther 2010;87:586–92.
[39] Brouwer OR, Van Den Berg NS, Mathéron HM, Wendler T, Van Der Poel HG, Horenblas S, et al. J Urol 2014;192:1810–6.